Ionic Liquids in Vacuo: Analysis of Liquid Surfaces Using Ultra–High–Vacuum Techniques

5 **AUTHORS**, INCLUDING:

Emily F Smith
University of Nottingham
19 PUBLICATIONS **482** CITATIONS

SEE PROFILE

Frank J M Rutten
Keele University
54 PUBLICATIONS **742** CITATIONS

SEE PROFILE

Peter Licence
University of Nottingham
117 PUBLICATIONS **3,735** CITATIONS

SEE PROFILE

Ionic Liquids in Vacuo: Analysis of Liquid Surfaces Using Ultra-High-Vacuum Techniques

Emily F. Smith,[†] Frank J. M. Rutten,[‡] Ignacio J. Villar-Garcia,[†] David Briggs,[‡] and Peter Licence*,[†,§]

School of Chemistry, School of Pharmacy and Centre for Surface Chemical Analysis, and School of Chemical, Environmental and Mining Engineering (SChEME), The University of Nottingham, Nottingham NG7 2RD, United Kingdom

Received May 4, 2006. In Final Form: August 10, 2006

Ultra-high-vacuum (UHV)-based techniques can offer the scientist a tremendous amount of information about samples of interest. However, until recently the range of samples that could be routinely investigated using unmodified instrumentation was limited to solid samples and frozen solutions. In this paper we report the investigation of low-vapor-pressure, liquid samples using both X-ray photoelectron spectroscopy and time-of-flight secondary ion mass spectrometry. We demonstrate the suitability of UHV techniques in the investigation of a range of room-temperature ionic liquids, offering the opportunity to measure high-quality solution-phase spectra using unmodified instrumentation.

Introduction

Over the past 35 years, many attempts have been made to successfully apply the powerful ultra-high-vacuum (UHV) techniques of the surface scientist to the study of the liquid–gas interface. During this time, many elegant experiments have been conducted on a range of aqueous[1] and nonaqueous solutions including inorganic acids.[2] Techniques developed over this period include the introduction of liquid samples using continually moving, wetted wires,[3] rotating disks,[4] and free-flowing macroscopic jets.[5] Unfortunately, none of the aforementioned techniques have been demonstrated to be universally applicable. In the case of X-ray photoelectron spectroscopy (XPS), for instance, the use of liquid jets and liquid-coated moving wires using instruments constructed around custom-designed vacuum chambers has been successful with a limited range of low-vapor-pressure liquids. Furthermore, very precise adjustment of the jet/wire position relative to the spectrometer slit is required to ensure that the liquid surface spectrum is not convoluted with that representative of the rapidly expanding vapor phase.[6] In all cases, the key problem that has to be overcome in the investigation of many traditional liquid samples is the extremely high evaporation rate of traditional liquid samples, which places an unacceptably large load on the pumping system employed to maintain collision-free conditions within the analytical chamber. More recently, experiments coupling liquid microjets with in vacuo surface-specific or -sensitive probes have been shown to be more successful; consequently, reports detailing this type of interface are becoming much more common in the literature.[5,7]

The problem of high evaporation rates does not apply to a particular class of liquids, namely, those that have vapor pressures that are comparable to or lower than the base pressures maintained within a UHV analytical chamber. A broad class of liquids with this property are room-temperature ionic liquids (RTILs).[8,9] In the broadest terms, RTILs are sterically hindered organic salts that have melting points below 100 °C. Because they are composed entirely of ions, they exhibit extremely low vapor pressures and do not evaporate, even under UHV.[10,11] In general, RTILs have a large liquid range, sometimes up to 300 °C (when compared to just 100 °C for water) and are both chemically and thermally stable to elevated temperatures.[12] This makes them particularly attractive as alternative solvents in the area of biphasic catalysis and in broader terms green chemistry. It has only been recently realized that the rather unusual combination of physical properties exhibited by RTILs allows them to be used in commercially available UHV systems without the requirement for either customized instrumentation or specialist sample handling systems.[13–15]

In this paper we seek to demonstrate the possibilities of RTIL-based samples for analysis by both XPS and static (time-of-flight, ToF) secondary ion mass spectrometry (SIMS) through a study of the experimental fundamentals: sample handling, sample conductivity, and surface purity. Representative spectral information from a number of ionic liquids is presented and discussed. Finally, the ability to investigate the transition from the liquid to the solid state, through sample cooling, is also demonstrated.

* To whom correspondence should be addressed. E-mail: peter.licence@nottingham.ac.uk.
† School of Chemistry.
‡ School of Pharmacy and Centre for Surface Chemical Analysis.
§ School of Chemical, Environmental and Mining Engineering (SChEME).

(1) Winter, B.; Faubel, M. *Chem. Rev.* **2006,** *106* (4), 1176–1211.
(2) Fairbrother, D. H.; Somorjai, G. A. *J. Phys. Chem. B* **2000,** *104* (19), 4649–4652.
(3) Fellner-Feldegg, H.; Siegbahn, H.; Asplund, L.; Kelfve, P.; Siegbahn, K. *J. Electron Spectrosc. Relat. Phenom.* **1975,** *7* (5), 421–428.
(4) Siegbahn, H.; Svensson, S.; Lundholm, M. *J. Electron Spectrosc. Relat. Phenom.* **1981,** *24* (2), 205–213.
(5) Wilson, K. R.; Rude, B. S.; Catalano, T.; Schaller, R. D.; Tobin, J. G.; Co, D. T.; Saykally, R. J. *J. Phys. Chem. B* **2001,** *105* (17), 3346–3349.
(6) Lundholm, M.; Siegbahn, H.; Holmberg, S.; Arbman, M. *J. Electron Spectrosc. Relat. Phenom.* **1986,** *40* (2), 163–180.

(7) Kondow, T.; Mafune, F. *Annu. Rev. Phys. Chem.* **2000,** *51,* 731–761.
(8) Welton, T. *Coord. Chem. Rev.* **2004,** *248* (21–24), 2459–2477.
(9) Wasserscheid, P.; Welton, T. *Ionic Liquids in Synthesis*; Wiley-VCH: Weinheim, Germany, 2002; p 364.
(10) Zaitsau, D. H.; Kabo, G. J.; Strechan, A. A.; Paulechka, Y. U.; Tschersich, A.; Verevkin, S. P.; Heintz, A. *J. Phys. Chem. A* **2006,** *110* (22), 7303–7306.
(11) Paulechka, Y. U.; Zaitsau, D. H.; Kabo, G. J.; Strechan, A. A. *Thermochim. Acta* **2005,** *439* (1–2), 158–160.
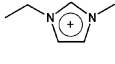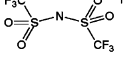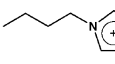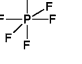(12) Fredlake, C. P.; Crosthwaite, J. M.; Hert, D. G.; Aki, S.; Brennecke, J. F. *J. Chem. Eng. Data* **2004,** *49* (4), 954–964.
(13) Smith, E. F.; Garcia, I. J. V.; Briggs, D.; Licence, P. *Chem. Commun.* **2005** (45), 5633–5635.
(14) Höfft, O.; Bahr, S.; Himmerlich, M.; Krischok, S.; Schaefer, J. A.; Kempter, V. *Langmuir* **2006,** *22,* 7120–7123.
(15) Caporali, S.; Bardi, U.; Lavacchi, A. *J. Electron Spectrosc. Relat. Phenom.* **2006,** *151* (1), 4–8.
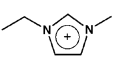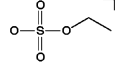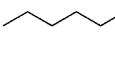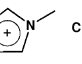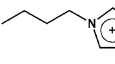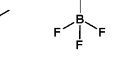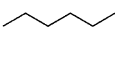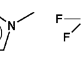
Table 1. Structures and Abbreviated Names of RTIL Samples Investigated during This Work

	[EMIM][NTf$_2$]			[BMIM][PF$_6$]
	[EMIM][EtSO$_4$]			[OMIM][Cl]
	[BMIM][BF$_4$]			[OMIM][PF$_6$]

Experimental Section

Materials. Unless otherwise stated, RTIL samples investigated during this study were either purchased from the Merck Chemical Co. or Solvent Innovations or prepared in our laboratory via established synthetic methods. The purity of all RTIL samples was independently assessed using ^{1}H NMR and ^{13}C NMR spectroscopy and Karl Fischer titration before use. The structures of the RTILs investigated are detailed in Table 1.

XPS. XPS spectra were recorded using a Kratos Axis Ultra spectrometer employing a monochromated Al Kα X-ray source ($h\nu$ = 1486.6 eV), hybrid (magnetic/electrostatic) optics, a hemispherical analyzer, a multichannel plate, and a delay line detector (DLD) with a collection angle of 30° and a takeoff angle of 90°. The X-ray gun power was set to either 100 or 150 W, dependent on the quality of the vacuum obtained. Unless otherwise indicated, all spectra were recorded using an aperture slot of 300 × 700 μm^2 with a pass energy of 80 eV for survey scans and 20 eV for high-resolution core-level scans. All XPS spectra were recorded using the Kratos VISION II software; data files were translated to VAMAS format and processed using the CASAXPS software package (version 2.3.2 and later). During the experiments, no charge compensation was used and the samples were earthed via the stage using a standard BNC connector.

Cooling experiments were carried out using standard Kratos stage cooling methods, employing liquid nitrogen as the coolant. The temperature of the stage was monitored using a mounted thermocouple in contact with the sample stub; however, some thermal lag should be expected because the thermocouple is not directly in contact with the RTIL sample. During low-temperature experiments, particularly when the sample is frozen, charge compensation was employed to check that the stoichiometry and peak shapes were nominally unchanged.

Prior to analysis, the RTIL samples were stored over indicating silica gel crystals in a vacuum desiccator. The samples (~0.5 mL) were presented for analysis using standard Kratos powder stubs. The RTIL samples were transferred onto the stubs using a small spatula. Sample pumping times were recorded to assess the suitability of each sample; rough pumping was carried out in an external airlock before being introduced into the main analytical chamber. In general, pumping times were rapid, achieving the required airlock vacuum (~5 × 10^{-7} Torr) after 30–60 min. The base pressure of the analytical chamber was typically 3 × 10^{-9} Torr during the experiments.

ToF-SIMS. All ToF-SIMS spectra were recorded on a ToF-SIMS IV instrument (ION-TOF GmbH, Münster, Germany) equipped with a single-stage reflectron analyzer. Ga$^+$ primary ions accelerated to 25 keV were rastered across a 200 × 200 μm^2 area, resulting in a dose of 10^{11} ions/cm^2, ensuring static conditions. Droplets of the ionic liquid were presented on the surface of clean Al foil, and a Mo grid was used to ensure that a flat liquid surface was presented to the primary ion beam, resulting in spectra with a topography-limited mass resolution (defined as $m/\Delta m$) of better than 6500. The mass scale was calibrated using a number of well-defined and easily assigned secondary ions (CH$_2$, C$_2$H$_2$, C$_3$H$_2$, and C$_4$H$_2$ in the positive spectrum, CH$_2$, C$_2$H, C$_3$H, and C$_4$H in the negative spectra). This allowed for assignment of the main ionic liquid fragments based on their absolute mass. Cooling experiments were carried out using an
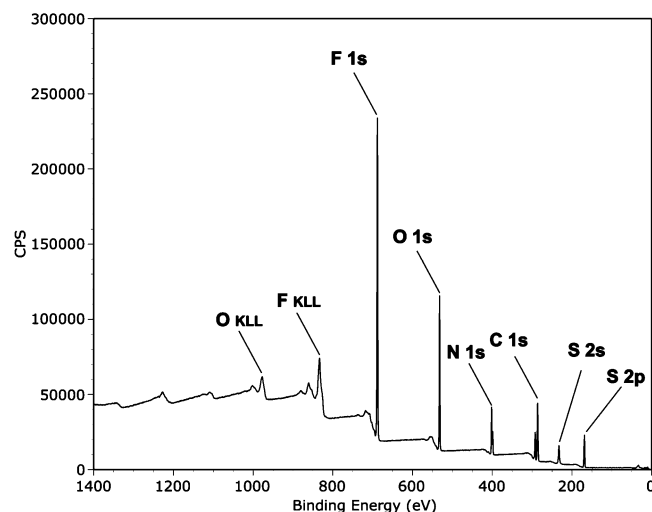

Figure 1. Survey scan XPS spectrum for the ionic liquid [EMIM]-[NTf$_2$].

ION-TOF variable-temperature stage employing liquid nitrogen as the coolant. The temperature of the stage was monitored using a thermocouple mounted in close proximity to the RTIL sample, thereby minimizing any temperature lag. As with the XPS experiments outlined above, sample pumping times were rapid. The required airlock vacuum (~2 × 10^{-6} Torr) was achieved after 20–30 min, and the base pressure of the SIMS chamber was typically 5 × 10^{-8} Torr during the experiments.

Results and Discussion

XPS. Under our analysis conditions, liquid RTILs emit a good photoelectron flux; hence, excellent XPS data can be obtained in a very short collection time (~5 min); see, for example, Figure 1. RTILs appear to be very stable during exposure to the X-ray source: we have observed no evidence of either outgassing, after initial pump-down, or beam damage to the sample. There is also no visible discoloration of the sample, which is common in many other organic-based samples, including polymers. Particular aspects of spectral features are discussed in the following paragraphs.

Sample Conductivity. Representative examples of XPS spectra of [EMIM][NTf$_2$] recorded in both survey (wide scan) and high-resolution (narrow scan) modes are shown in Figures 1 and 2, respectively. In all cases, survey spectra are recorded with excellent resolution, with fwhm values for both the N 1s (Figure 2a) and C 1s (Figure 2b) components being as low as 1.0 eV. In addition, the spin–orbit-coupled S 2p doublet (Figure 2d) is also observed with high resolution. These data were all obtained without the requirement for charge compensation, indicating that the RTILs studied behave as electrical conductors under the experimental XPS conditions. This was confirmed by the
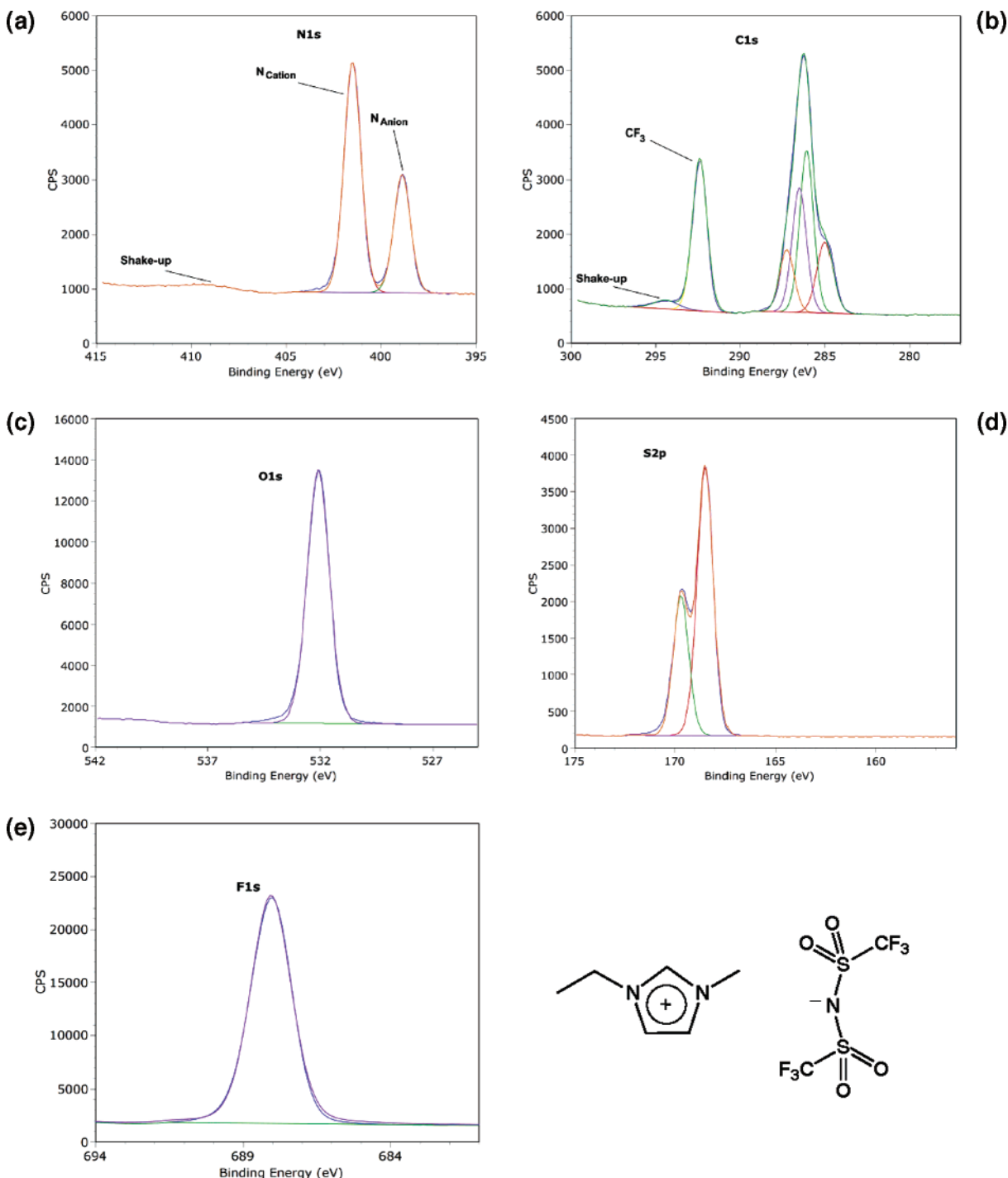
Figure 2. Representative high-resolution XPS spectra for each of the atomic constituents in the RTIL [EMIM][NTf$_2$].

application of a bias voltage (9 V) to the sample holder; XPS spectra recorded under these conditions were indeed observed to be shifted by the applied voltage.

In the specific case of [EMIM][NTf$_2$] a section of the edge of the sessile drop was imaged to reveal a surrounding precursor film of 100−200 μm width. Using a 110 μm diameter aperture, selected area spectra were acquired from within the bulk of the droplet, from within the precursor film (with spectral components from both the RTIL and the Au stub), and from the clean Au stub, well away from the film-covered region. The film thickness was clearly well below the sampling depth of the Au 4d and 4f electrons, since these were hardly attenuated relative to the "bare" substrate. In this thin-film situation even an inherently insulating material would behave as a conductor during XPS. To within

0.05 eV there were no absolute binding energy (BE) differences between the core-level spectra from the different regions, a further indication that the bulk liquid is behaving as an electrical conductor.

Dependence of Conductivity on Changes of State. A sample of [EMIM][EtSO$_4$] was slowly cooled in situ while the C 1s peak was continuously monitored. The peak shape remained unchanged until the liquid drop showed signs of freezing, whereupon the peak suddenly distorted and lost intensity before disappearing from the scanned region. Clearly, the sample was now charging. Switching on the charge compensation filament immediately returned the peak to a position close to the scanned energy range and restored the peak shape. Each component is returned to a position approximately 2 eV below that observed in the conducting
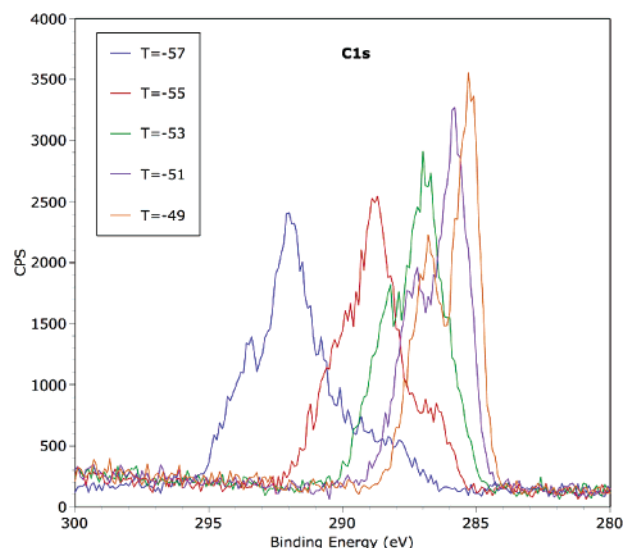
Figure 3. High-resolution XPS spectra showing the measured binding energy of the C 1s photoemission as a function of temperature. At lower temperatures, when the sample becomes frozen, surface charging occurs and the band is observed to shift to a higher energy.

state; this shift can be attributed to slight overcompensation by the filament, i.e., negative charging of the surface. This observation is consistent with experiments carried out on polymer systems and other poorly conducting organic-based solids.

The nature of the solid−liquid transition can be better observed by reversing this process, i.e., monitoring the behavior of the spectrum as the prefrozen sample is warmed, since this allows for significantly better temperature control. Figure 3 shows the C 1s region acquired at regular intervals as the sample was allowed to warm from −57 to −49 °C (as indicated by the stage thermocouple). Below −57 °C the peak was completely distorted and essentially outside the scanned region, while above −49 °C there was no further change in the peak position or shape.

It should be noted that the conductivity of RTILs is known to be attenuated by subtle variations in the concentration of water.[16,17] Careful measurements of the relative positions of a peak representing the liquid (e.g., F 1s) and the gold substrate (Au 4f) indicted statistically significant differences in reproducibility (e.g., at different points on the samples and/or at different times) depending on the length of time a sample had been in the vacuum system and consequently the concentration of water present. Typically, an initial reproducibility on the order of ± 0.2 eV would be improved to ± 0.02 eV after several weeks of pumping. This behavior may well be explained by a slow reduction in the concentration of water in the drop and testifies to the extremely low vapor pressure of the RTIL itself.

Quantification. Quantification of spectra using the relative sensitivity factors (RSFs) in the Kratos data processing software gave only reasonable agreement with the known atomic compositions of the RTIL samples (Table 2). However, in all cases except that of [EMIM][EtSO$_4$], the deviation from the

theoretical stoichiometry gave little cause to suspect substrate surface contamination. Surface bombardment with Ar$^+$ has been shown to remove surface contamination. Interestingly, we have seen no evidence of further contamination at the surface, even over prolonged periods of time (up to 7 h), suggesting that the contaminant is not present in the bulk liquid.

The derivation of the Kratos sensitivity factors is not documented, although it is believed that they have been adapted from early values published by Wagner et al.[19] Consequently, a systematic series of experiments were carried out to generate a set of modified, experimentally determined RSFs from a series of RTILs of high purity (>99%). Fluorine-containing anions are especially suited for this purpose because (i) they facilitate direct reference to the F 1s photoemission, which has RSF = 1 (by convention), and (ii) the atoms involved in emissive processes are not affected by shake-up/off events, which are often observed in the case of unsaturated or aromatic species including imidazolium cations; see below. Thus, measurement of the [NTf$_2$] anion allows the determination of RSFs for C 1s, N 1s, O 1s, and S 2p, while investigation of [BF$_4$] and [PF$_6$] anions provides values for B 1s and P 2p, respectively. Experimentally determined RSFs and, for comparison, those available within the Kratos data system are given in Table 3; these values may be used in comparative studies as the relative peak areas employed in their derivation have been subjected to transmission function correction.

Occasionally, traces of silicone were also detected in the survey scan spectra (maximum Si concentration of 2 atom %) despite great care being taken to avoid such contamination during sample mounting for XPS examination. In these cases the contamination is believed to be inherent, i.e., introduced during preparation and not during sample mounting for analysis.

Curve-Fitting. Fitting of the C 1s envelope is illustrated in Figure 4 for [BMIM][BF$_4$] since contributions come only from the [BMIM] cation. The equivalent carbons are numbered in the structure and identified with the four components in the fitted peak. For all components a Gaussian−Lorentzian product function with 30% Lorentzian was used to model the peak shape with the fwhm's constrained to 0.9−1.1 eV. The binding energy positions of the three components C^1−C^3 were fixed relative to each other such that BE(C^1−C^2) = 0.43 eV and BE(C^1−C^3) = 1.17 eV. The final component (C^4) represents atoms in alkyl chains, and BE(C^3−C^4) is around 2.5 eV (varying by ± 0.25 eV; see below). The peak areas for C^1−C^3 were fixed in the ratio 0.8:1.6:2.0. This recognizes the losses due to shake-up/off from the intensities of the aromatic ring carbons (C^1 and C^2). The shake-up peaks can be clearly seen in Figure 4, and their combined intensity is approximately 10% of that of the ring carbons. An equivalent loss was assumed for shake-off,[20] leading to the ratios reported above. The ratio of peak areas for C^4 and C^3 is 3:2, in agreement with the calculated stoichiometry of these carbon types. This fitting protocol is consistently successful across all six ionic liquids measured, and it differs somewhat from a preliminary report based only on [EMIM][EtSO$_4$],[13] where the envelope is further complicated by additional components from the [EtSO$_4$] anion.

The model highlighted above is simplified with respect to the peak shape that is applied to each of the synthetic components used in the construction of the model. In particular, the saturated alkyl chain carbons will give rise to a vibrationally broadened, nonsymmetric peak shape.[21] This effect becomes more significant

(16) Jarosik, A.; Krajewski, S. R.; Lewandowski, A.; Radzimski, P. *J. Mol. Liq.* **2006**, *123* (1), 43−50.

(17) Widegren, J. A.; Saurer, E. M.; Marsh, K. N.; Magee, J. W. *J. Chem. Thermodyn.* **2005**, *37* (6), 569−575.

(18) Shake-up/shake-off is due to the excitation of π orbital electrons by exiting photoelectrons, either into a higher energy bound state or into the continuum. This leads to a loss of energy from the main peak and the appearance of a broader, less well defined peak at a lower kinetic energy/higher binding energy. Note there is also a contribution to the background; this however is not easily measurable. (See also: Briggs, D., Seah, M. P., Eds. *Practical Surface Analysis, Vol 1, Auger and X-Ray Photoelectron Spectroscopy*; John Wiley and Sons: Chichester, U.K., 1994.).

(19) Wagner, C. D.; Davis, L. E.; Zeller, M. V.; Taylor, J. A.; Raymond, R. H.; Gale, L. H. *Surf. Interface Anal.* **1981**, *3* (5), 211−225.

(20) Beamson, G.; Briggs, D. *Mol. Phys.* **1992**, *76* (4), 919−936.

(21) Beamson, G.; Clark, D. T.; Kendrick, J.; Briggs, D. *J. Electron Spectrosc. Relat. Phenom.* **1991**, *57* (1), 79−90.

Table 2. Peak Quantification (Expressed as Concentration, atom %) for Each Element Present in the RTIL Samples Investigated during This Work

	concn,[a] atom % (theory)					
	[EMIM][EtSO$_4$]	[EMIM][NTf$_2$]	[BMIM][BF$_4$]	[BMIM][PF$_6$]	[OMIM][Cl]	[OMIM][PF$_6$]
C 1s	67.3[b] (53.3)	34.7 (34.8)	51.0 (53.3)	51.2 (47.1)	81.0 (80.0)	56.0 (57.1)
C 1s[c]	1.3	[d]	2.0	1.4	1.6	2.0
N 1s	8.8 (13.3)	12.4 (13.0)	12.1 (13.3)	11.8 (9.4)	12.0 (13.3)	8.8 (9.5)
F 1s		29.6 (26.1)	28.6 (26.7)	33.3 (35.3)		30.3 (28.6)
B 1s			6.5 (6.7)			
P 2s				4.7 (5.8)		3.9 (4.7)
O 1s	18.4 (26.6)	16.0 (17.4)				
S 2p	4.2 (6.7)	7.3 (8.7)				
Cl 2p					5.5 (6.7)	

[a] Calculated from high-resolution scans of each photoemission by applying the standard Kratos sensitivity factors. [b] Clear evidence of hydrocarbon contamination. [c] Additional contribution of C 1s due to shake-up.[18] [d] The contribution due to shake-up was not calculated for this example simply because the shake-up band coincided in energy with that of the shifted C contribution arising from the trifluoromethyl (CF$_3$) substituent found within the [NTf$_2$] anion.

Table 3. Empirically Derived RSFs for Use in the Quantification of Solution-Phase XPS

	empirically derived RSF[a]	Kratos RSF		empirically derived RSF[a]	Kratos RSF
F 1s	1.00	1.00	O 1s	0.60	0.78
B 1s	0.14	0.16	P 2p	0.40	0.49
C 1s	0.26	0.28	S 2p	0.49	0.67
N 1s	0.39	0.48			

[a] A full account of the experimental details of the derivation of empirical RSFs for liquid samples will be reported elsewhere.
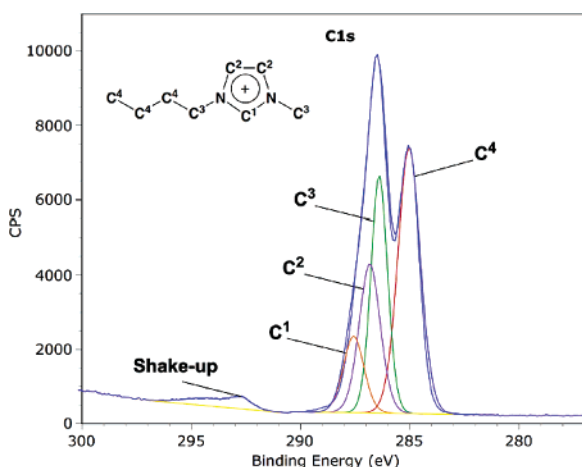

Figure 4. High-resolution XPS spectrum of [BMIM][BF$_4$], detailing the C 1s photoemission. The experimental data (blue) are compared to a simulated fit where each nonequivalent carbon atom had a distinct shift in binding energy. For all components a Gaussian–Lorentzian product function with 30% Lorentzian was applied with fwhm's constrained to 0.9–1.1 eV.

as the relative proportion of this contribution increases.[22] The enforcement of a symmetric peak shape to all components, together with fixed relative positions of C^1–C^3, is largely responsible for the apparent variation in the relative position of the C^4 component. However, although much simplified, this methodology offers an excellent first approximation that may be used in the interpretation of our experimental data.

Shake-up is also observed for the N 1s peak representing the imidazolium ring nitrogen atoms (Figure 2). The structure is broad and less well defined than is the case for the equivalent C 1s feature, partly because the intensity is lower. The shake-up:main peak intensity ratio is about 6% for the samples studied. For [EMIM][NTf$_2$] the intensity of the two main N 1s components

(22) Briggs, D.; Fairley, N. *Surf. Interface Anal.* **2002**, *33* (3), 283–290.

Table 4. Comparative BEs for a Series of RTILs Using C 1s (C^1) as an Internal Reference

	C 1s BE (eV)			imidazolium N 1s BE (eV)
	C^1	C^4	C^1–C^4	
[EMIM][NTf$_2$]	287.64	285.40	2.24	401.93
[EMIM][EtSO$_4$]	287.64	285.20	2.44	402.05
[BMIM][PF$_6$]	287.64	285.00	2.64	402.14
[BMIM][BF$_4$]	287.64	285.10	2.54	401.91
[OMIM][Cl]	287.64	285.29	2.35	401.96
[OMIM][PF$_6$]	287.64	284.90	2.74	402.00

is close to the stoichiometric ratio of 2:1. Shake-up involving the N component of the anion is not expected to be significant, so a deficit in the ring N component intensity would be anticipated (as for the C 1s peak).

BEs and Chemical Shift Referencing. Given the conducting nature of the liquids, absolute BE data would be ideal for comparisons since this would allow possible relaxation effects to be investigated. However, small variations in the efficiency of grounding of the sample can lead to errors unless this is checked by measurements of the type described above, namely, the simultaneous measurement of the liquid drop, the film on a conducting substrate, and the otherwise bare substrate. Experiments of this type are nontrivial and as such are extremely time-consuming. At this time, we compare the RTILs using an internal reference derived from a single experiment of this type performed on [EMIM][NTf$_2$]/Au. For Au 4f$_{7/2}$ BE = 84.00 eV, for the C 1s ring component due to N–C–N (C^1) BE = 287.64 eV, and for the C 1s component due to C–C–C (C^4) BE = 285.40 eV. This latter BE is expected to be close to 285 eV (frequently used for energy referencing of insulating materials), but the error in this value, described above, will probably be high for this compound since the relative intensity of the C^4 component is the lowest of all the liquids studied. Using instead the N–C–N (C^1) C 1s BE as an internal reference for comparisons between the liquids leads to the data shown in Table 4. Note that the mean value for the C^4 component is close to the expected value of 285 eV (285.15 ± 0.25 eV). Within experimental error the N 1s BE is constant at 402.0 ± 0.1 eV. The C1s curve fits can all be accomplished without any relative change in the C^1–C^3 positions, as noted previously. Thus, the evidence from relative core-level BEs and shake-up intensities suggests that any effect of variation in the attached alkyl groups on the electronic structure of the imidazolium ring is slight. Absolute BE data are required to comment on possible effects relating to cation–anion interactions. This will be an area of future study using pairs of liquids with common components and synthetic mixtures.
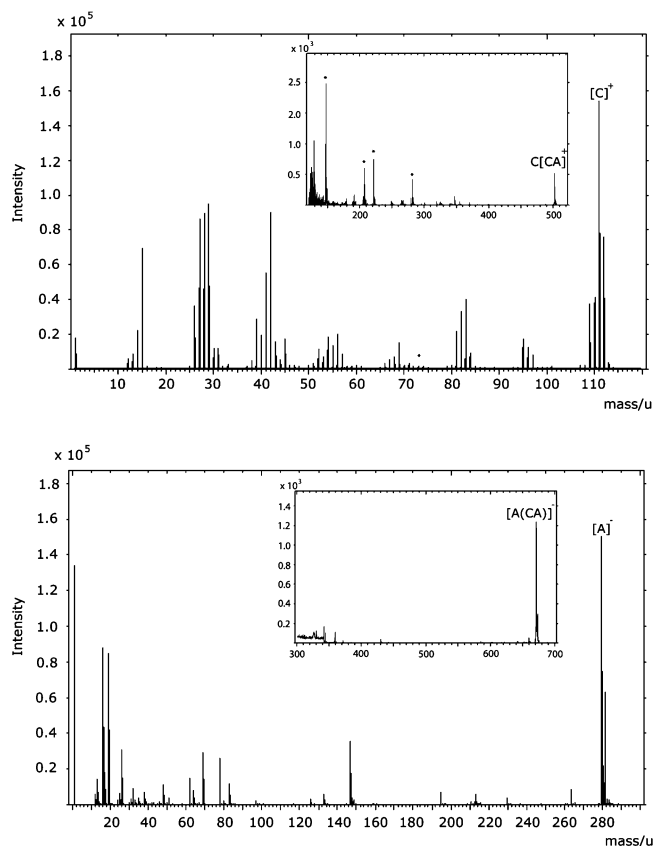
ToF–SIMS. The top and bottom panels of Figure 5 show representative SIMS spectra from [EMIM][NTf$_2$], recorded in

Figure 5. ToF-SIMS spectra recorded for [EMIM][NTf$_2$] dominated by contributions from intact anions and cations, in both negative and positive polarities, respectively. Higher molecular mass clusters of general formulas [C(CA)$_n$]$^+$ and [A(CA)$_n$]$^-$, where $n = 1$, are observed in both positive and negative polarities; see the insets. Peaks annotated by an asterisk are associated with trace PDMS contamination.

both positive and negative polarities, respectively, with each spectrum displaying the mass range containing the main peaks of interest. A trace of the almost ubiquitous contaminant poly-(dimethylsiloxane) (PDMS) is present as indicated (*) in the positive spectrum; however, both spectra are clearly dominated by RTIL-related peaks. The most intense positive ion peak is that of the intact [EMIM] cation, but significantly weaker peaks associated with [EMIM] fragment ions are also observed. Peaks corresponding to the loss of alkyl CH$_x$ fragments, presumably leaving the imidazolium ring intact, and lower molecular weight fragments resulting from cleavage of the aromatic ring itself are also observed. In the negative ion spectrum, the intact [NTf$_2$] anion is still very prominent and most of the negative fragments can readily be explained by single-bond cleavage of the intact anion fragment. Fragments including CF$_3$SO$_2$ are especially notable above mass 132, where all prominent fragments include this moiety. Ionic solids, both organic and inorganic, give rise to cluster ions of generic formulas [C(CA)$_n$]$^+$ and [A(CA)$_n$]$^-$ (C = cation, A = anion) in the positive and negative ion spectra, respectively. In the case of [EMIM][NTf$_2$], clusters where $n = 1$ are observed in both positive and negative polarities; see the insets in Figure 5.

ToF-SIMS spectra were also recorded for [EMIM][EtSO$_4$], which has a nominally higher viscosity at room temperature.[23] As in the case of [EMIM][NTf$_2$], the spectra are dominated by contributions from intact anions and cations, in both negative

(23) Jacquemin, J.; Husson, P.; Padua, A. A. H.; Majer, V. *Green Chem.* **2006**, *8* (2), 172−180.

and positive polarities, respectively. Expected fragmentation patterns and higher molecular weight cluster ions are also observed with notable negative fragments of general formula H$_x$SO$_y^-$ (where $x = 0$, 1 and $y = 1-4$). The positive spectrum is highly comparable as expected, and cluster ions are again observed for both polarities.

Interestingly, at room temperature the ionic liquids were shown to be sufficiently conducting as to not require charge compensation during data collection; this however was not the case at lower temperatures. Below a threshold temperature of ca. −90 °C, in the case of [EMIM][EtSO$_4$], no secondary ion signal could be generated without the provision of charge compensation, which was accomplished by supplying low-energy electrons (1 μA, 20 eV). During a temperature-ramped experiment, in which spectra were recorded at regular intervals while the sample stage was cryocooled and reheated, the observed transition in the conductive behavior of the sample was sharp and reversible and appeared to correspond to a phase change of the sample within the chamber. However, spectra recorded below this temperature were statistically indistinguishable from those collected at higher temperatures. It had been thought that from the solid material the yield of the complex cluster ions might increase (see below). However, attempts at X-ray diffraction on samples frozen under similar conditions showed that the solid formed was a noncrystalline glass. The lack of lattice formation is therefore consistent with the ToF-SIMS results. A general comparison that should be drawn at this point, however, is the accuracy of the measured sample temperatures obtained during the comparable SIMS and XPS experiments. We believe that monitoring of the sample stage temperature inside the SIMS instrument is far superior to that of the XPS spectrometer, hence the rather large temperature differential between the two experiments (ca. −90 and ca. − 54 °C, respectively). This does, however, by no means invalidate the XPS observations with regard to temperature-dependent solidification and charging, even though there is a significant error in temperature measurement.

General Discussion. In our first report of the application of XPS to study RTILs, we made a preliminary interpretation of the spectrum from [EMIM][EtSO$_4$] and discussed, in particular, the prospects for the study of dissolved inorganics important for RTIL-based homogeneous catalysis.[13] In this work we have attempted a much more systematic study of the XPS spectra of representative RTILs and the experimental factors which affect the results.

During the final stages of preparation of this paper, Caporali et al. reported XPS data for the single compound [BMIM][NTf$_2$],[15] a closely related homologue of [EMIM][NTf$_2$] included in this study. The relative core-level BEs are in good agreement (absolute values are dependent on the energy scale correction, which is not fully specified by Caporali et al.), as are the fitted components of the C 1s envelope. However, the authors have not recognized the existence of shake-up during emission from the atoms involved in the aromatic imidazolium ion. As we discussed in detail, this has significant consequences for quantification, especially of C 1s components during curve-fitting. Thus, calculation of RSFs on the assumption of stoichiometric peak intensities is not valid. In the case of compounds containing the [NTf$_2$] anion, the C 1s shake-up peak overlaps the CF$_3$ component, but with sufficiently high sensitivity and energy resolution it can easily be resolved. A comparison of Figure 2b with Figure 3 of Caporali et al. shows that the shake-up peak is actually just observable in the latter, but the counting statistics meant it went unrecognized. To quantify the difference in instrument characteristics leading to these two spectra, note that in the present work the count rates are 3 times

greater combined with an analyzer resolution of 0.56 eV for the $Ag_{5/2}$ fwhm (1.2 eV for Caporali et al). A very high signal-to-noise ratio, at high energy resolution, is clearly essential for these spectra to be correctly interpreted. More recently, Kempter et al. published an account of a complimentary series of experiments including a description of surface charging when [EMIM][NTf_2] is cooled below its glass transition temperature.[14] Further studies employing ultraviolet photoelectron spectroscopy (UPS) appear to confirm the presence of surfacial ordering, most specifically the orientation of the imidazolium moiety away from the surface. This observation may give rise to a time-resolved variation in observed stoichiometric ratios, i.e., lower C 1s contribution from the imidazolium when compared with larger aliphatic components.

We believe the ToF-SIMS spectra of RTILs are the first to be reported. The extremely intense peaks due to the cation and anion in the positive and negative ion spectra, respectively, are expected since ionization during sputtering is not required. A particularly interesting observation is the cluster ions of generic compositions $[C(CA)_n]^+$ and $[A(CA)_n]^-$ (C = cation, A = anion). For inorganic salts, especially the alkali-metal halides, cluster ions of this type are well-known. Static SIMS spectra of salts involving large organic cations or anions, typically surfactants/antistatic agents, have been reported, but in these cases only one of the ions is a "large" organic species (typically the counterion is either Na^+ or a halide ion).[24] The observation of high yields of cluster ions for [EMIM][NTf_2] (both the cation and anion organic are large) is therefore novel. These clusters offer a potential insight into ion association (or binding) in RTILs, through the study of mixtures. It is worth noting that these spectra were obtained using Ga^+ primary ions; using higher mass species such as SF_5^+ or multiatom metal clusters should lead to even higher yields of these useful secondary ions.

The electrical conductivity of RTILs is one of their many useful attributes. We have studied this here in relation to their behavior under ionization radiation. The overwhelming evidence from both the XPS and ToF-SIMS experiments reported is that the liquids behave as electrical conductors under these conditions, but that insulating behavior is observed as soon as the liquid is cooled to solidification. However, there are still aspects to be fully explored. Careful XPS measurements of the peak positions of both the liquid and solid states under electron irradiation (from the charge neutralizer) indicate subtle effects that are not yet

understood. Preliminary ToF-SIMS results from solidification of other RTILs suggest that the behavior reported for [EMIM][$EtSO_4$] may not yet be generalized.

Conclusions

We have shown that a range of powerful UHV surface analytical techniques can be successfully employed in the investigation of real liquid samples, consequently opening up a whole series of techniques that allow one to probe liquids in a novel way. XPS spectra, which probe the sample to a depth of ca. 10 nm, have been obtained from six representative RTILs under conditions of high sensitivity and high-energy resolution, allowing a detailed investigation of curve-fitting protocols. Shake-up affects photoemission from the imidazolium ring atoms, and this has important consequences for data quantification. Although the RTILs behave as electrical conductors under XPS conditions, the direct comparison of absolute binding energies is still uncertain and further work needs to be done on this aspect. Using an internal reference procedure, however, shows that the electron distribution within the imidazolium ring is little affected by either the alkyl substituents or the anion composition.

Two of the RTILs have also been studied by ToF-SIMS (a more surface selective technique with analysis depths of ca. 1−2 nm), and again, the behavior was typical of an electrical conductor. Intense peaks due to the cation and anion were observed, as expected, in the positive and negative ion spectra, respectively. Also observed were cluster ions of compositions $[C(CA)_n]^+$ and $[A(CA)_n]^-$. Although well-known for inorganic salts, the observation for salts with a large organic cation and anion, as in the case of [EMIM][NTf_2], is novel. This opens up interesting prospects for the study of ion association.

The behavior of [EMIM][$EtSO_4$] during cooling to a temperature below the solidification point has been studied by continuous observation during temperature-ramped experiments for both XPS and ToF-SIMS. In both cases a dramatic change was observed on solidification, such that the material now behaved as an electrical insulator and application of the normal "charge-neutralization" low-energy charge compensation was required for spectra to be recorded.

(24) *The Static SIMS Library*, version 3; SurfaceSpectra: Manchester, U.K., 2002.